Aerodynamics of a flapping wing as a function of altitude: New insights into the flight strategy of migratory birds Ⓕ ⓢⓒⓘ

ⓘⒹ Fabien Beaumont, Sebastien Murer, Fabien Bogard, et al.

COLLECTIONS

Ⓕ This paper was selected as Featured

ⓢⓒⓘ This paper was selected as Scilight

View Online   Export Citation   CrossMark

ARTICLES YOU MAY BE INTERESTED IN

Aerodynamics of a flapping wing as a function of altitude: New insights into the flight strategy of migratory birds Ⓕ ⓢⒸⒾ

View Online · Export Citation · CrossMark

Fabien Beaumont,[1,a)] ⒾⒹ Sebastien Murer,[1] Fabien Bogard,[1,2] and Guillaume Polidori[1] ⒾⒹ

AFFILIATIONS

[1]MATIM, Université de Reims Champagne-Ardenne, Reims, France
[2]Pôle de Recherche Châlonnais, Université de Reims Champagne-Ardenne, Châlons-en-Champagne, France

[a)]Author to whom correspondence should be addressed: fabien.beaumont@univ-reims.fr

ABSTRACT

Migratory birds have developed remarkable physiological and biomechanical adaptive capacities in order to fly at very high altitudes and benefit from favorable wind. Numerous studies suggest that increased frequency would be an adaptive mechanism of flapping flight in hypodense and hypobaric air. We sought to assess this hypothesis using a numerical model of the wing flapping kinematics of a migratory bird and an evaluation of the cyclic variation of aerodynamic forces as a function of altitude (100 to 4000 m). In an attempt to reproduce the variations in the thermophysical parameters of air vs altitude, subroutines have been implemented in a finite-volume-based code. Numerical results indicate a strong correlation between the intensity of forces exerted on the wing and the flight altitude. For instance, it has been shown that mean lift ranges from 2.63 N at 100 m to 0.76 N at 4000 m. In addition, the results suggest that increasing the flapping frequency to 5 Hz would induce a value of $(C_L/C_D)_{max}$ of 31.8, corresponding to a 158% increase compared to a flapping frequency of 4 Hz. Finally, this study aims at broadening current knowledge of the biomechanical mechanisms used by migratory birds to maintain a favorable balance between flight performance at high altitude and the energetic cost of the migration.

I. INTRODUCTION

During their annual migration, some birds choose flight altitudes based on a combination of criteria, such as minimal energy consumption and favorable tail and cross winds.[1] A number of migratory birds even climb to 9000 m in search of air currents that allow them to reach flight speeds above 45 m/s.[2] At these altitudes, the winds are undeniably stronger but the air density is lower. This variation causes, among other things, drastic changes in the aerodynamic and biomechanical behavior of the bird. The aerodynamics of a body strongly depends on the surrounding environment, and aerodynamic coefficients, such as drag and lift are proportional to air density.[3] Air density decreases with the increasing altitude, thereby reducing the aerodynamic drag forces that oppose the bird's motion, but also decreasing the lift force required for flight. For this reason, some birds are able to adjust their biomechanical behavior in response to the thermophysical properties of the air that vary with altitude.[4–6] For example, birds flying at high altitudes in low-density air (i.e., well below sea level) must increase the frequency and amplitude of their wing flapping[7–9] but also their flight speed to maintain sufficient lift force. The current state of knowledge

and hypotheses in this relevant area is based on visual observations of free-flying birds.[10,11] To date, there is a real lack of scientific evidence regarding the causal relationship between altitude, aerodynamics, and adaptation of biomechanical behavior of birds in flight (flapping speed, amplitude, and frequency). The main reason is that wind tunnel tests are very contentious on free-flying birds, they require specific training of the birds, and the use of an aerodynamic balance is impossible. Furthermore, in standard wind tunnels, the air density cannot be adjusted, although hypobaric chambers can be used to simulate altitude variations. Tucker[12] addressed a number of physiological issues related to high-altitude flight by studying oxygen consumption and transport in the circulatory system of birds. The primary focus of these experiments was to investigate the physiological adaptation of birds to altitude, while discarding aerodynamic aspects arising from variations in the physical parameters of the air. Even today, measuring aerodynamic coefficients on a flying bird remains a challenge, and the evolution of drag and lift forces is estimated using theoretical mathematical models and flapping kinematic analysis. Nafi et al.[13] used particle image velocimetry

(PIV) and a hypobaric climatic wind tunnel to study the aerodynamic forces acting on three several bird species (wader, songbird, and barn owl) in free flight. However, these forces were evaluated by a mathematical method based on experimental measurements in the bird's wake, and on the momentum equation for viscous flows. Such a procedure is necessary because it is impossible to implement an aerodynamic balance system on a bird in free flight. Numerical simulation, and more precisely computational fluid dynamics (CFD), has proven to be an interesting and efficient alternative to study the aerodynamics of fixed or flapping wings.[14–16] Among the CFD studies performed in this relevant field, some have focused on the geometrical parameters of the wing,[17] others on the effects of the ceiling[18] or the ground,[19] but none seem to have addressed the effects of altitude on the aerodynamics of a flapping wing. The CFD method has shown great flexibility in simulating various experimental conditions, and the accuracy of its results is now considered sufficient.[20,21]

Although many studies assume a strong link between aerodynamics and biomechanical adaptation of flapping flight in migratory birds, a review of the relevant literature shows that there is a real lack of scientific evidence. This study aims to fill this gap by estimating the aerodynamic forces exerted on the wing of a barnacle goose as a function of flight altitude (between 100 and 4000 m).

Bird wings provide almost all the aerodynamic forces required for flight, although the body and tail can be used for flight control and lift enhancement.[22] Based on this statement and the assumption that the flow in the wake is symmetric with respect to the bird's body,[23] modeling the kinematics of a single wing seems sufficient as a first approach to the aerodynamic performance of the bird in flapping flight. In order to demonstrate a relationship between aerodynamics and biomechanical adaptation during flight, two flapping frequencies (4 and 5 Hz), two amplitudes (50 and 60 cm), and two speeds (14 and 17 m/s) were tested. The evolution of the thermophysical parameters of the air as a function of altitude is taken into account through subroutines implemented in the code. The dynamic behavior of a goose wing is modeled using a CFD computational code based on the finite volume method.

A. Calculation of air properties as a function of altitude

Several parameters likely to affect the aerodynamics of the flight evolve according to the altitude, such as the temperature and the absolute hygrometry of the air, the density, and the viscosity but also the atmospheric pressure or the acceleration of the gravity.

B. Acceleration of gravity as a function of altitude

$$g(h) = g_0 \left(\frac{R_e}{R_e + h} \right)^2, \tag{1}$$

with $g_0 = 9.79 \, \text{m s}^{-2}$ (g-value at the equator), $g(h)$ acceleration of gravity at altitude $h(m)$ above sea-level, R_e mean radius of Earth ($\cong 6.378 \times 10^6 \, \text{m}$).

In the altitude range of interest, i.e., [100–4000 m], $g(h)$ does not vary significantly (only to the second decimal place).

C. Density of air as a function of atmospheric pressure

As with the partial pressure of oxygen, the density of air systematically decreases with altitude, proportionally to the associated change in total pressure. Air density at sea-level and at a temperature of 20 °C is about $1.21 \, \text{kg/m}^3$, decreasing to $1 \, \text{kg/m}^3$ at 2000 m and $0.81 \, \text{kg/m}^3$ at 4000 m, the latter corresponding to a reduction of 32% compared to the value at sea-level.

The following equation gives the value of air density as a function of atmospheric pressure P_{atm} (Pa), temperature T (K), and relative humidity H_r. Coefficient R_S is equal to 287.058 J kg^{-1} K^{-1}.

$$\rho = \frac{1}{R} \frac{P_{atm}}{T} = \frac{\left(1 - \frac{0.3783 \, H_r \, P_{sat}(t)}{P_{atm}}\right) P_{atm}}{R_S T}. \tag{2}$$

Throughout this study and for simplification purposes, it will be assumed that relative humidity H_r remains constant, regardless of altitude ($H_r = 60\%$).

D. Atmospheric pressure as a function of altitude

$$p(h) = 101\,325 \times \left(1 - 2.255\,77 \times 10^{-5} \, h\right)^{5.255}. \tag{3}$$

The relationship between the dynamic viscosity of air μ (Pa s) and the temperature T (K) is given by Sutherland's semi-empiric law,

$$\mu(T) \approx \mu(T_{ref}) \left(\frac{T}{T_{ref}} \right)^{3/2} \frac{T_{ref} + S}{T + S}, \tag{4}$$

where $T_{ref} = 273.15$ K (reference temperature), $S = 110.4$ K (numerical constant related to the selected gas), and $\mu(T_{ref}) = 1.715 \times 10^{-5}$ Pa s.

II. NUMERICAL METHODS

A. Geometry and computational domain

The simplified wing geometry [Fig. 1(a)] was created using ANSYS Worbench Design Modeler® CAD software and from the real shape of a Canada goose wing in flight.[24,25] The values for wingspan and maximum chord are 0.72 and 0.3 m, respectively (see Table I). The actual wings of birds are very flexible, and flapping involves not only up and down movements, but also twisting and folding movements. In this study, which focuses on the effects of altitude on the aerodynamics of the wing, the wing will be considered as a rigid, undeformable solid body (see Fig. 1).

The distance between the wing and the boundaries of the computational domain was defined in accordance with the recommendations issued by the CFD best practice guide.[26] According to these guidelines, the blockage ratio is less than 3. The dimensions of the computational domain as well as the boundary conditions are presented in Fig. 1.

B. Boundary conditions

A constant velocity of 14 m/s was imposed at the entrance to the computational domain, which corresponds to the average flight speed of barnacles during their migratory flight.[14,25,27] At the exit of the computational domain, a pressure boundary condition was selected, which defines a flow condition based on the flow pressure at the exit. This boundary condition is selected when the flow reaches a fully developed state where no change occurs in the flow direction and when the outlet is selected away from geometric disturbances. In such a region, an
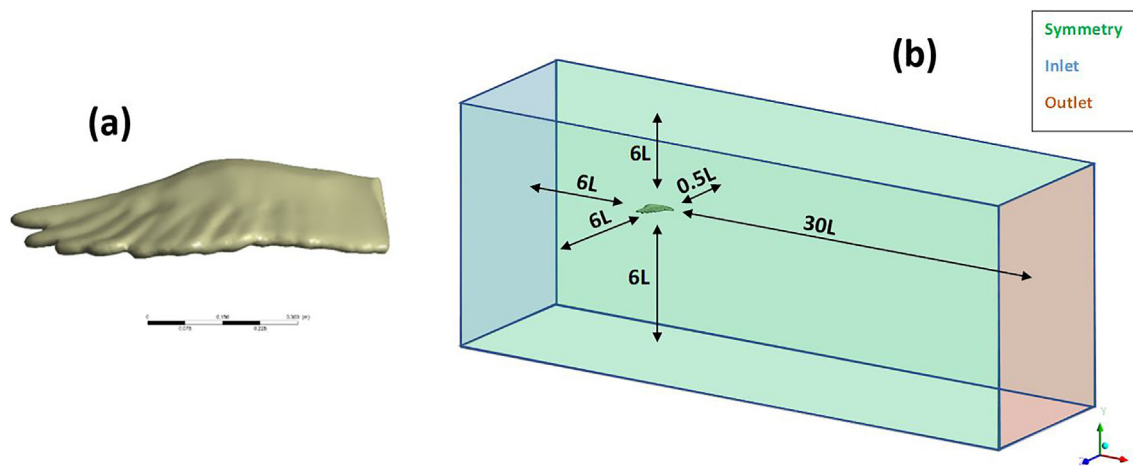
FIG. 1. (a) Simplified geometry of goose wing; and (b) computational domain size and boundary conditions.

outlet can be defined and the gradient of all variables can be zero in the flow direction except for pressure. A symmetry condition was used for the top, bottom, and side surfaces of the computational domain. This boundary condition can be used when the physical geometry and the expected flow pattern exhibit mirror symmetry. The use of symmetry conditions reduces the size of the computational domain and therefore the computational cost. In this case, the CFD code assumes a zero flux of all quantities across the symmetry boundary: the component normal to the symmetry plane is, therefore, zero. In addition, to account for altitude variations, user-defined functions (UDFs) have been implemented in the code to model the evolution of the thermophysical parameters of the air (see Sec. II). Gravitational acceleration and atmospheric pressure evolve during the simulation as a function of altitude using analytical expressions also implemented in the code (Table I).

C. Modeling of the flapping motion

In this study, modeling of the wing flapping motion was performed based on the wing flapping dynamics of a bird in flight[24] (see Fig. 2). The motion is complex and involves several rotational motions, each of which has an influence on the mechanics of flight. To simplify the model and improve numerical convergence, the wing was assumed to be a rigid body whose motion consists of a single rotation about the x-axis (Fig. 2). Therefore, the rotation of the leading edge of the wing

will be neglected, which affects the value of the thrust force. The average flapping frequency in Canada geese is around 4 Hz (Refs. 27 and 28) but is likely to vary with altitude.[7,29,30] Real-time modeling of wing flapping required the use of an adaptive dynamic mesh, capable of updating the wing position at each time step ($\Delta t = 0.001$ s).

The volumetric mesh update is performed automatically by the Fluent© solver, and the method is based on a local remeshing based on interpolation and adapted to large and complex displacements. This dynamic meshing method allows the wing trajectory to be determined by the aerodynamic or hydrodynamic forces of the surrounding flow field. In addition, the diffusion-based smoothing algorithm was used to move the mesh nodes in response to the boundary shift. This algorithm calculates a mesh velocity using a diffusion equation, i.e., the velocity at the boundary nodes is used as a Dirichlet boundary condition. In addition, the local face remeshing method marked the faces (and adjacent cells) on the deformation boundaries based on their asymmetry. The wing trajectory (i.e., flapping amplitude and

TABLE I. Characteristic values.

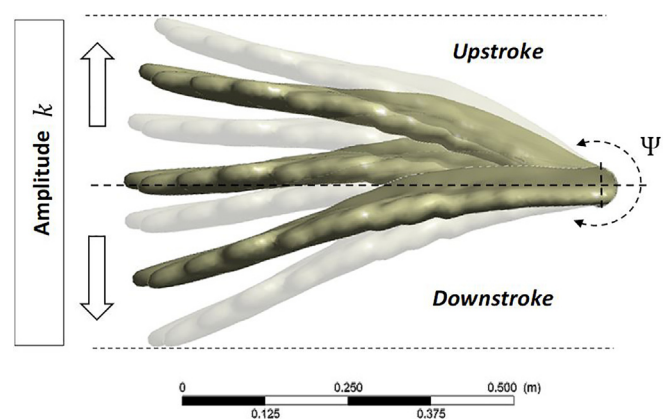| Parameter	Value
Flapping amplitude k	50 and 60 cm
Wingbeat frequency f	4 and 5 Hz
Velocity u	14 and 17 m/s
Max wing chord C_{max}	0.3 m
Wingspan L	0.72 m

FIG. 2. Reconstitution of the wing position over a complete stroke. Wing motion comprises a main rotation about the x axis. Both the frequency and amplitude of flapping are implemented via subroutines.

TABLE II. Total number of cells for each of the tested meshes, average cell size in the wing wake and computation time for 250 time steps of 0.001 s.

	Total cells	Mesh size in the wake	CPU time
Coarse mesh	3.1×10^4	0.075 m	4 h 12 min
Medium mesh	6×10^4	0.050 m	6 h 36 min
Refined mesh	9.8×10^4	0.025 m	10 h 13 min

frequency), which consists of a top–down rotation, was implemented in the code using user-defined functions (UDFs).

Wing rotation Ψ is defined as follows:

$$\Psi(t) = k.\cos(2\pi f). \quad (5)$$

D. Meshing methods

The three-dimensional, unstructured mesh of the computational domain was created using ANSYS Workbench Meshing$^©$ software. To test the independence of the mesh size on the results, three grid sizes were tested. The size of the elements in the near-wing wake, the total number of cells, as well as the computation time for 250 time steps are shown in Table II. In addition, we have plotted in Fig. 3 the time evolution of the lift and drag coefficients for the three tested grids.

We can see that the evolution of the lift coefficient values during a flapping cycle is relatively similar for the medium and refined meshes while the values are higher for the coarse mesh. The same conclusions can be drawn for the evolution of the drag coefficient. Finally, the results obtained with the medium mesh are very close to those obtained with the refined mesh. Considering the computational time required for each of the tested grids, we selected the medium mesh for all the calculations, as it presents the best ratio of computational time/accuracy of results. Figure 4 shows both the surface mesh of the wing and the three-dimensional mesh shown in a vertical transverse plane. As shown in Fig. 4, a very fine mesh was generated at the boundary layer (i.e., near the wall) to obtain accurate results in the viscoelastic and laminar sublayer.[31] In addition, to better reproduce the boundary layer separation, a inflation layer consisting of 15 sublayers of increasing thickness (growth rate: 1.2) was generated around the wing boundary [Fig. 4(a)]. To obtain the value of y^* close to 1 that is essential for
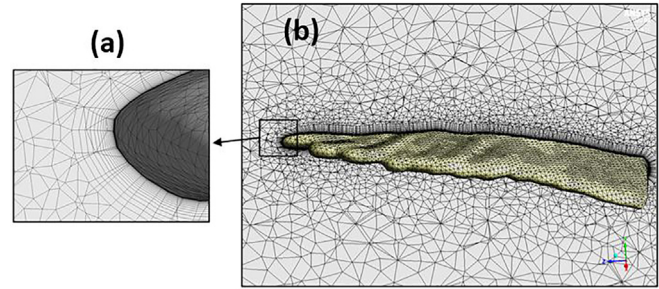

FIG. 4. Detailed view of the inflation mesh around the wing (a); and Surface mesh on the wing and in a vertical plane intersecting the bird wing (b).

accurate boundary layer resolution, the cell size adjacent to the bird's wing wall is 10 μm. In addition, a mesh refinement zone was created around and within the wing wake to capture major physical phenomena, such as shear layers and vortex structures. Outside this area, the mesh becomes coarser to reduce the number of elements, and thus the computation time.

E. Simulation setup

Unlike incompressible flows for which density changes can be neglected, the present problem involves altitude changes that affect both the density and viscosity of the fluid. Therefore, turbulent flow is governed by the Reynolds-averaged Navier–Stokes (RANS) equations for compressible flows.[32]

Assuming conservation of mass, the continuity equation is written as follows:

$$\frac{\partial \rho}{\partial t} + \nabla \cdot (\rho u) = 0. \quad (6)$$

The compressible momentum Navier–Stokes equation can be expressed as follows:

$$\frac{Du}{Dt} = \rho \left(\frac{\partial u}{\partial t} + u \cdot \nabla u \right)$$

$$= -\nabla \overline{p} + \nabla \cdot \left\{ \mu \left(\nabla u + (\nabla u)^T - \frac{2}{3} (\nabla \cdot u)I \right) \right\} + \rho g, \quad (7)$$
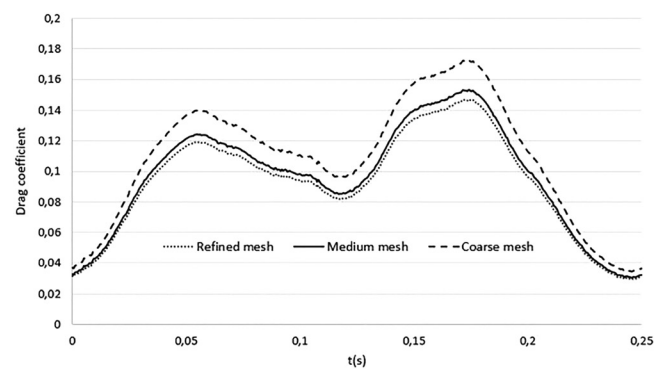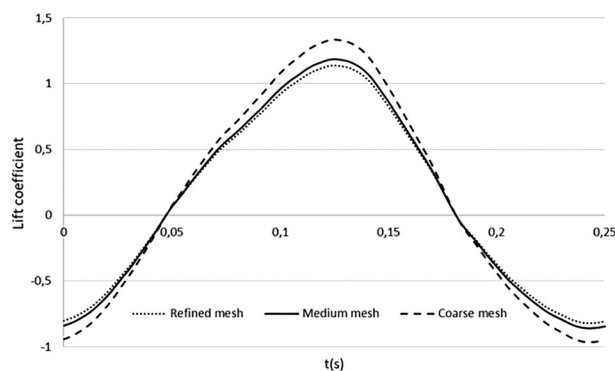

FIG. 3. Variation of lift and drag coefficients during one flapping cycle for the three tested meshes.

where ρ is the density, μ the dynamic viscosity, u the flow velocity, $\nabla \cdot$ the divergence, p the pressure, t the time, and g the gravity.

The calculations were performed using the CFD code ANSYS Fluent[©] 2020 R2. The SST k–ω model (Menters Shear Stress Transport turbulence model) was chosen to solve the RANS (Reynolds-averaged Navier–Stokes) equations in 3D.[33] The SIMPLE algorithm was used for the pressure–velocity coupling and the gradients calculated by the least squares cell-based method. In order to investigate the influence of the order of accuracy of the numerical scheme, comparative simulations were performed using the first- and second-order upwind schemes. The results showed that the temporal evolution of the lift coefficient during a wing flapping cycle was similar regardless of the order of accuracy of the numerical scheme. Regarding the evolution of the drag coefficient, only a slight difference was found in the maximum value obtained between the upstroke and downstroke phases; note that this difference was less than 6% and limited to a particular moment of the flapping cycle.

As a result, the first-order upwind scheme was chosen because it decreases the computational time. The SST k–ω turbulence model is a two-equation eddy-viscosity model that is currently used in a variety of relevant fields ranging from industry to sports.[31] It is a hybrid model combining the capabilities of the k–ω and k–ε models, allowing for a gradual transition from the standard k–ω model in the inner region of the boundary layer to a high-Reynolds-number version of the k–ε model in the outer part of the boundary layer. The k–ω SST model provides a better prediction of flow separation than most RANS models and achieves optimal performance under adverse pressure gradients due to its ability to account for the transport of the principal shear stress.[21,34]

The SST $k - \omega$ model has a similar form to the standard $k - \omega$ model,

$$\frac{\partial}{\partial t}(\rho k) + \frac{\partial}{\partial x_i}(\rho k x u_i) = \frac{\partial}{\partial x_j}\left(\Gamma_k \frac{\partial k}{\partial x_j}\right) + \tilde{G}_k - Y_k + S_k, \quad (8)$$

and

$$\frac{\partial}{\partial t}(\rho \omega) + \frac{\partial}{\partial x_i}(\rho \omega u_i) = \frac{\partial}{\partial x_j}\left(\Gamma_\omega \frac{\partial \omega}{\partial x_j}\right) + G_\omega - Y_\omega + D_\omega + S_\omega. \quad (9)$$

$\tilde{G}_k$ represents the generation of turbulence kinetic energy due to mean velocity gradients. G_ω represents the generation of ω and Γ_k and Γ_ω are, respectively, the effective diffusivity of k and ω. Y_k and Y_ω represent the dissipation of k and ω due to turbulence, D_ω is the cross-diffusion term, and S_k and S_ω are user-defined source terms.

The drag and lift coefficients, as well as the air density, kinematic viscosity, and atmospheric pressure, were monitored at each time step, which was set to $\Delta t = 0.001$ s. Computations were performed on a Dell Precision 7920 workstation and parallelized on 48 Xeon Gold CPUs (3.2 GHz). Given the value of Δt, there are about 250 time steps for each wing flapping at 4 Hz and 200 time steps for each wing flapping at 5 Hz.

F. Aerodynamic forces

There are four forces acting on an object or animal in flight, whether it is a bird, a bat, an insect, or an airplane: lift, thrust, drag, and gravity. With the exception of the hummingbird, birds generate lift and thrust by flapping their wings: a complex, unsteady, three-dimensional motion that varies with each new wing position.[35] Wing flapping consists of two phases: the downstroke, or powerstroke, which creates most of the thrust; and the upstroke, or recovery stroke, which generates a certain amount of thrust depending on the shape of the wing.[36] Of course, wings create not only lift and thrust forces, but also drag. Lift and drag are two components of the resultant aerodynamic force acting on the wing,[37] the magnitude of which depends primarily on the stroke velocity.[36] The lift force can act in any direction relative to gravity, since it is defined relative to the direction of flow rather than gravity. In horizontal flight, most of the lift force is opposed to gravity.[38] However, during climb, descent, or change of direction, the lift force is tilted with respect to the vertical direction.

The most significant parameters in wing stroke aerodynamics are the drag (C_D) and lift (C_L) coefficients, defined as follows:

$$C_D = \frac{F_D}{\frac{1}{2}\rho U^2 A}, \quad (10)$$

$$C_L = \frac{F_L}{\frac{1}{2}\rho U^2 A}, \quad (11)$$

where F_D and F_L are the drag and lift forces, respectively; ρ is the fluid density, U is the forward velocity, and A is the projected area (m^2).

III. RESULTS AND DISCUSSION
A. Validation

The results of the calculations for an altitude of 100 m and a velocity between 14 and 17 m/s showed that the minimum drag coefficient is between 0.03 and 0.046, and the maximum lift coefficient varies between 1.07 and 1.2. These values are relatively close to those of the experimental study by Withers,[39] which showed that bird wings have high minimum drag coefficients (0.03–0.13) and low maximum lift coefficients (0.8–1.2).

B. Wing flapping kinematics

The evolution of the lift and drag coefficients during two wing flapping cycles for an altitude of 100 m is shown in Fig. 4, the position of the wing at several moments of the cycle being represented by letters. Figure 5 shows that these two coefficients vary throughout the wingbeat cycle which is composed of two phases: the upstroke (ascending motion) and the downstroke (descending motion).

The maximum value of the positive lift coefficient is about 1.2, while the negative value (upstroke) is −0.8. A significant decrease in drag coefficient is observed when the lift coefficient reaches its maximum value, at mid-downstroke. It is also interesting to note that the aerodynamic force is mainly produced during the downstroke. In addition, the upstroke also provides a fraction of the lift or thrust forces required during flight.

C. Evolution of drag and lift forces as a function of altitude

During their annual migration, some birds fly at altitudes that allow them to minimize their energy expenditure. However, the progressive decrease in air density as altitude increases has harmful consequences on the aerodynamic forces exerted on the bird's body. A lower air density leads to a decrease in the forces acting on
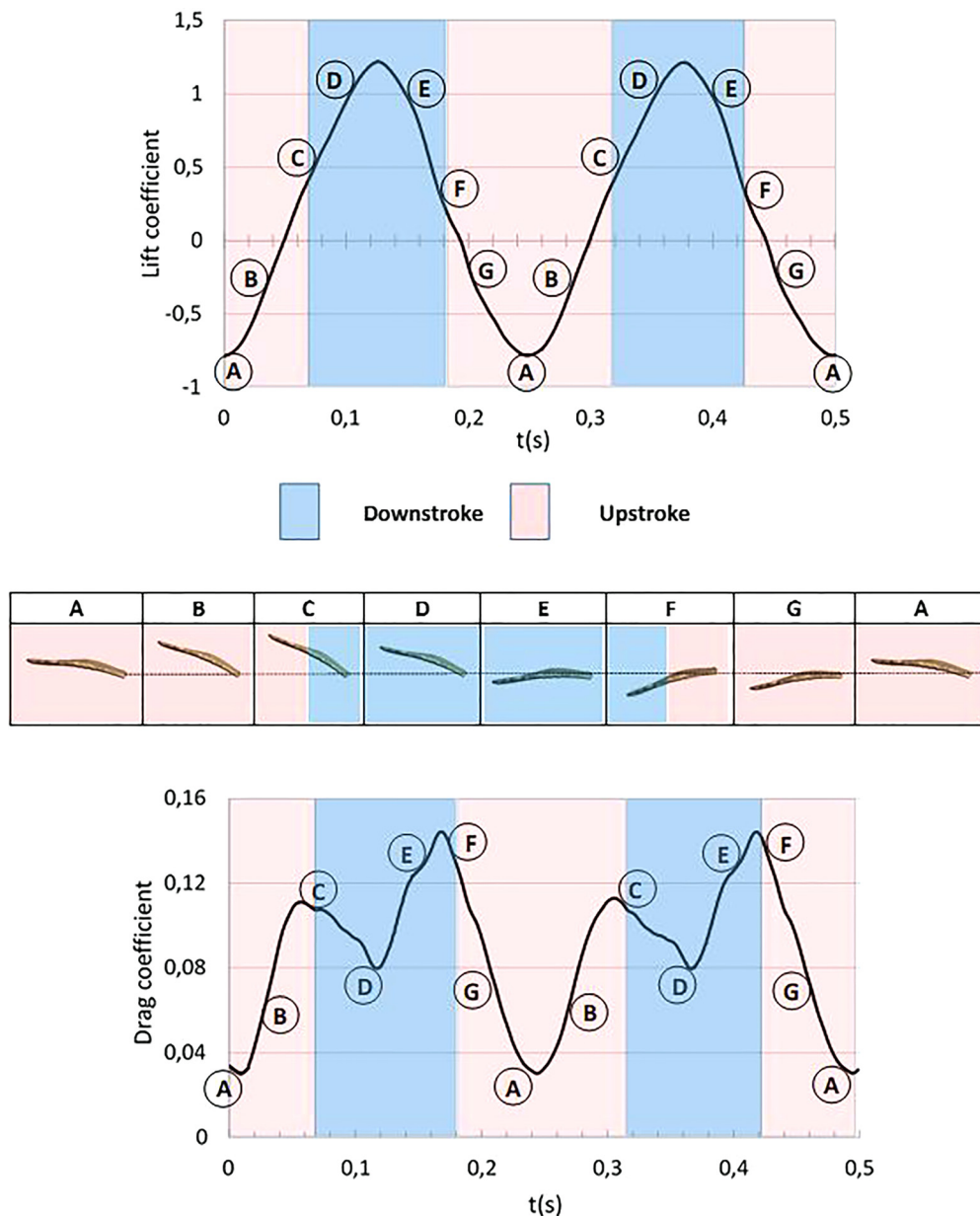
FIG. 5. Variation of lift and drag coefficients during two consecutive wing strokes ($u = 14\,\text{m/s}$, $k = 50\,\text{cm}$, $f = 4\,\text{Hz}$). The downstroke and upstroke movements are colored blue and red, respectively. The letters refer to the position of the wing at different instants of the flapping cycle.

the wings while the kinematics of flight (i.e., the speed, amplitude, and frequency of flapping) remain unchanged. To better highlight the relationship between altitude and aerodynamic forces applied to the wing, a first calculation was performed with a constant speed of 14 m/s. Figure 6 shows the evolution of the aerodynamic coefficients during a full wing stroke, presented in a C_D/C_L phase diagram. The trajectory can be assimilated to a closed orbit, which is in agreement with the assumption of a periodic flow. It can also be noted that the lift coefficient is an order of magnitude larger than

the drag coefficient.[40] The trajectory maintains a butterfly shape, regardless of the altitude.

Figure 7 shows the evolution of lift and drag coefficients for a flight altitude ranging from 100 to 4000 m. Several relevant information can be deduced from these figures. First, as shown in Fig. 5, the value of the coefficients evolves periodically during the flapping cycle of the wing with values that are either positive or negative as a function of the wing stroke. Second, the results show that the flight altitude has a significant influence on the aerodynamic forces exerted on the wing:
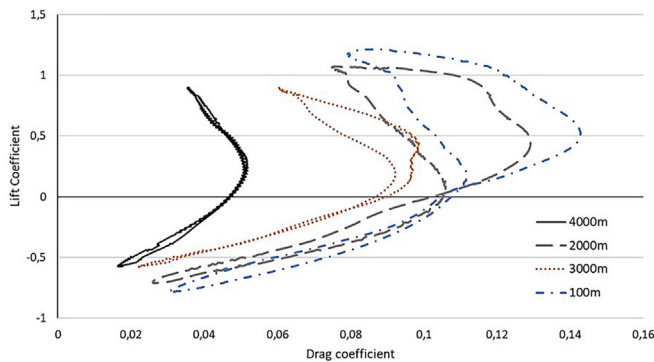
FIG. 6. drag vs lift coefficients over one stroke for various altitudes ($u = 14$ m/s, $k = 50$ cm, $f = 4$ Hz).

the higher the bird flies, the lower the forces exerted on its body. For example, the maximum value of the lift coefficient decreases from 1.2 at 100 m to 0.38 at 4000 m. The drag coefficient decreases drastically with a maximum value of 0.14 at 100 m while it is 0.04 at 4000 m. To facilitate the comparison between several cases, the drag and lift forces were averaged over a wing stroke. The average lift force at 100 m is 2.63 N, and it drops to 0.76 N at 4000 m, which is a decrease in 71% between these two altitudes. The average drag force is estimated to be 1.11 N at 100 m, but increasing the altitude to 4000 m results in a 72% decrease in this value ($\overline{L} = 0.29$ N).

Lift and drag forces are directly related to the density, viscosity, and compressibility of the air surrounding the aerodynamic profile surfaces. Between 100 and 4000 m, the density of the air decreases by
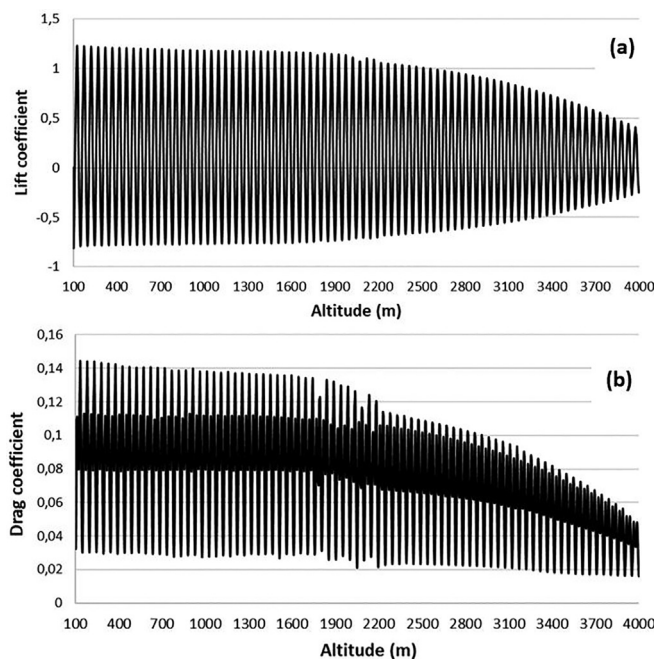

FIG. 7. (a) Lift coefficient vs altitude ($u = 14$ m/s, $k = 50$ cm, $f = 4$ Hz). (b) Drag coefficient vs altitude ($u = 14$ m/s, $k = 50$ cm, $f = 4$ Hz).

32% and the atmospheric pressure by more than 38%, while other parameters, such as viscosity and acceleration of gravity, vary in lesser proportions (6 and 0.12%, respectively). According to the theory, any object immersed in a viscous fluid flow experiences a net force due to the shear stresses and pressure gradients arising from the fluid motion. In this study, the physical parameters of the fluid (air) are constantly changing with flight altitude. Consequently, it seems important to take into account the combined effects of pressure, viscosity, density, and velocity gradients in the analysis of the aerodynamic performance of the wing. Based on this observation, it can be assumed that the aerodynamic forces acting on the wing depend on all the thermo-physical parameters of the air, not only on its density, which may partly explain why the lift and drag forces decrease by more than 70% between 100 and 4000 m.

D. Wing stroke frequency

It can be seen in Fig. 7 that the progressive decrease in air density as altitude increases is beneficial in reducing the aerodynamic drag forces that oppose the movement of the bird. The disadvantage of high-altitude flight is that the lift force required to maintain flight is degraded. For this reason, birds have adapted their biomechanical behavior to changes in altitude.[5,6,10] For example, birds flying at high altitudes in hypodense air increase both the frequency and amplitude of their wing strokes.[29,30] It has been reported that increasing the frequency of wing strokes is the most common mechanism adopted by birds to compensate for the decrease in lift at high altitudes.[11]

In order to estimate the influence of wing stroke frequency on the aerodynamic forces acting on the wing, we performed a second calculation. The results obtained for the two selected frequencies (i.e., 4 and 5 Hz) are presented for comparison in Fig. 8. The baseline results (altitude: 100 m, stroke frequency: 4 Hz) are also reported. It appears that a 25% increase in frequency (i.e., 4 to 5 strokes per second) produces a 28% increase in average lift force. At the same time, the drag decreases by 14%.

E. Air velocity

According to Hedenström et al.,[9] the increase in velocity is proportional to $(\rho_0/\rho)^{1/2}$, where ρ_0 represents the density of the air at the reference altitude (100 m above sea level in the present study) and ρ its value at the current altitude (ranging from 100 to 4000 m above sea level). In other words, the flight speed increases by about 5% for every 1000 m increase in altitude. With a speed of 14 m/s at an altitude of 100 m, the bird would fly at 17 m/s at 4000 m. The evolution of lift and drag forces at an altitude of 4000 m for two several speeds (14 and 17 m/s) are presented in Fig. 9, the results obtained with a speed of 14 m/s at 100 m are displayed for comparison. It appears that at an altitude of 4000 m, the increase in the flight speed from 14 to 17 m/s produces an increase in 45% of the average lift force. Unfortunately, the average drag force increases in the same proportion, and its value is going from 0.29 to 0.45 N.

F. Wing flapping amplitude

In addition to the biomechanical adaptations discussed above, birds sometimes amplify their wing stroke amplitude.[29,30] Additional results obtained with a wing stroke amplitude of 60 cm were compared to those obtained with an amplitude of 50 cm. As shown in Fig. 10, for
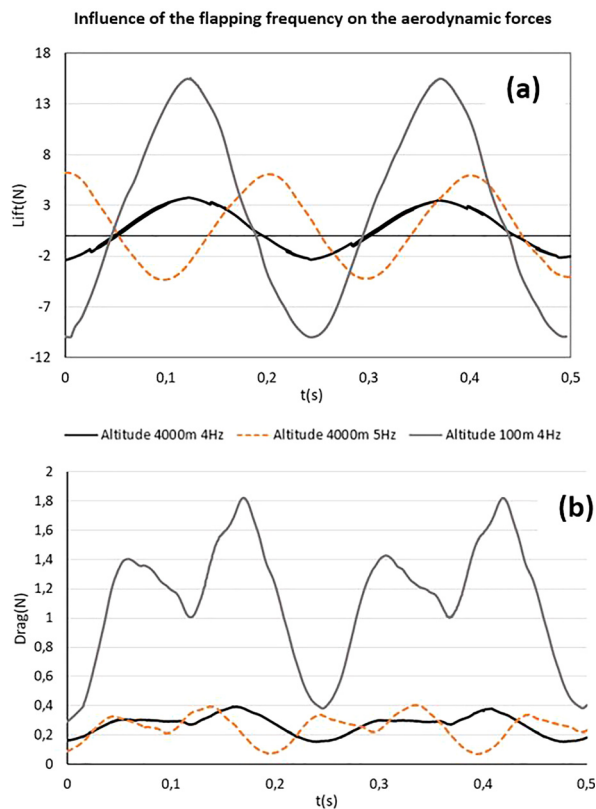
FIG. 8. (a) Lift force vs time over two wing strokes at altitudes 100 and 4000 m ($u = 14\,\text{m/s}$, $k = 50\,\text{cm}$, $f = 4$ and 5 Hz). (b) Drag force vs time over two wing strokes at altitudes 100 and 4000 m ($u = 14\,\text{m/s}$, $k = 50\,\text{cm}$, $f = 4$ and 5 Hz).

FIG. 9. (a) Comparison of lift force evolution over two wing strokes at altitude 100 m and velocity $u = 14\,\text{m/s}$ vs altitude 4000 m and two velocities $u = 14$ and 17 m/s ($k = 50\,\text{cm}$, $f = 4\,\text{Hz}$). (b) Comparison of drag force evolution over two wing strokes at altitude 100 m and velocity $u = 14\,\text{m/s}$ vs altitude 4000 m and two velocities $u = 14$ and 17 m/s ($k = 50\,\text{cm}$, $f = 4\,\text{Hz}$).

a flapping frequency of 4 Hz, a 10-cm increase in flapping amplitude (50 to 60 cm) results in an 83% increase in average lift force (0.76 to 1.39 N). However, the drag force also increases by a similar amount [see Fig. 10(b)].

G. L/D ratio

Our results highlight a close relationship between the biomechanics of wing flapping, altitude and aerodynamic forces exerted on the wing. The purpose of this study is to examine the effects of altitude on the aerodynamics of a bird's wing, as well as the biomechanical mechanisms used to maintain sufficient lift force at high altitude. The highest aerodynamic efficiency is achieved by improving lift and reducing drag forces, meaning that an unfavorable drag force requires additional energy expenditure, thus reducing the efficiency of the wing. For a quantitative comparison of the strategies used by birds in terms of altitude adaptation, we focused on the L/D ratio.

In aerodynamics, the lift to drag ratio L/D is the amount of lift generated by a wing divided by the aerodynamic drag created as the wing moves through the air. Higher values of this ratio mean that the wing is producing lift with a lower drag force, which is a favorable situation and one of the main indicators of lower energy expenditure. In other words, optimizing the biomechanics of flight will allow the bird to fly longer distances at the same energy cost.
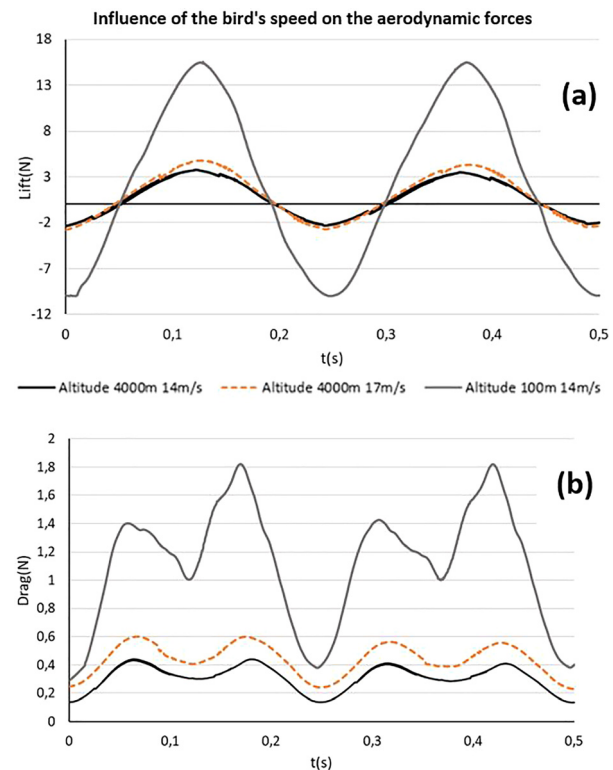
Figure 11 represents the evolution of the L/D ratio during a wing flapping cycle for two different flapping frequencies (4 and 5 Hz), two amplitudes (50 and 60 cm) and two speeds (14 and 17 m/s), for an altitude of 4000 m. At a flight speed of 17 m/s (frequency 4 Hz, amplitude 50 cm), the value of the ratio $(C_L/C_D)_{\max}$ is around 11.7 while it reaches 12.3 at 14 m/s. This result indicates that the increase in velocity induces a higher energy expenditure, since an increase in airflow velocity implies higher power output levels.[41] On the other hand, increasing the amplitude of the wingstroke (50 to 60 cm) leads to a significant improvement in the L/D ratio with a value of $(C_L/C_D)_{\max}$ of 15, a gain of 22% compared to an amplitude of 50 cm. The most striking observation is related to the flapping frequency: at 5 Hz, the value of $(C_L/C_D)_{\max}$ reaches 31.8, an increase in 158% compared to the baseline value (14 m/s, 4 Hz). This remarkable gain is most likely overestimated given the wing flapping frequencies reported in the literature. Bishop *et al.*[8] measured this parameter in bar-headed geese and showed that the frequency is altitude dependent, with a mean value of 3.94 Hz below 2300 m and 4.35 Hz above 4800 m. Although the frequency of 5 Hz chosen in this study is higher than those in the literature, our results suggest that increasing flapping frequency is the most effective biomechanical adaptation mechanism to allow birds to maintain sufficient lift for high-altitude flights. Such flights allow them to benefit from favorable winds, thus minimizing the energetic cost of migration.
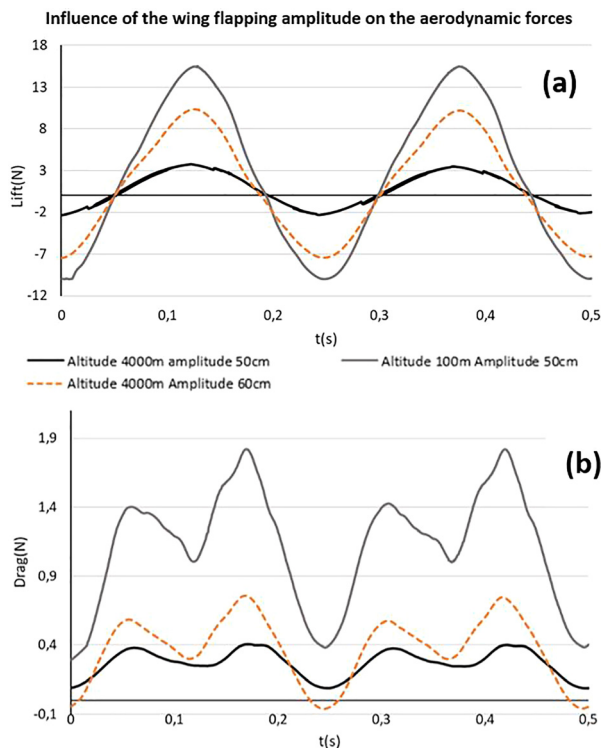
FIG. 10. (a) Comparison of lift force evolution over two wing strokes at altitude 100 m ($u = 14$ m/s, $k = 50$ cm) vs altitude 4000 m and two wing stroke amplitudes $k = 50$ and 60 cm. (b) Comparison of drag force evolution over two wing strokes at altitude 100 m ($u = 14$ m/s, $k = 50$ cm) vs altitude 4000 m and two wing stroke amplitudes $k = 50$ and 60 cm.

IV. CONCLUSION

In this study, the kinematics of a flapping bird wing was modeled to estimate the cyclic variations of the aerodynamic forces as a function of the flight altitude (between 100 and 4000 m). In order to reproduce the evolution of the thermo-physical parameters of the air with
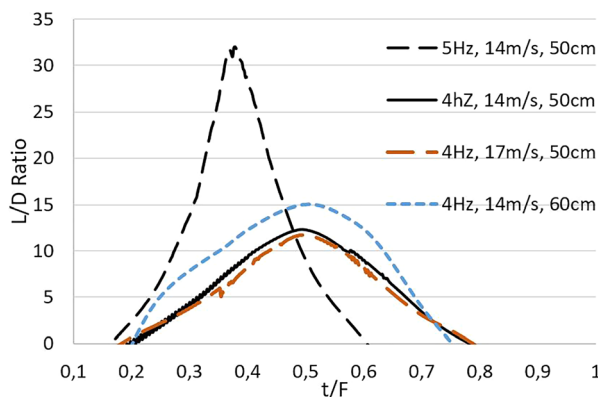

FIG. 11. Comparison of L/D ratio at an altitude of 4000 m and a flapping frequency f of 4 and 5 Hz, velocity u of 14 and 17 m/s and wing stroke amplitude k of 50 and 60 cm.

altitude, subroutines were implemented in a computational code based on the finite volume method. As altitude increases, atmospheric parameters related to air pressure, viscosity, and density affect drag and lift forces during flight. Between 100 and 4000 m, air density decreases by 32%, atmospheric pressure by 38%, and viscosity by 6%, while lift and drag forces decrease by 71 and 72%, respectively. Therefore, it seems important to consider the combined effects of these factors when analyzing flight performance. Flying at high altitude is beneficial since the drag force that opposes forward motion is drastically reduced, but on the other hand, the lift force that allows the bird to fly is also decreased. In this article, several biomechanical mechanisms that allow birds to maintain sufficient lift during high-altitude flight were discussed. Among them, increasing the wing stroke by 10 cm (from 50 to 60 cm) increases the average lift force by 83%, the value increasing from 0.76 to 1.39 N. Unfortunately, the drag force is also increased by a similar amount. A decrease in drag force allows birds to fly faster, and increasing the flight speed from 14 to 17 m/s at an altitude of 4000 m would increase the average lift force by 45%. Yet the average drag force would increase by a comparable amount, from 0.29 to 0.45 N. Numerous studies suggest that birds increase their wing stroke frequency to compensate for the decrease in lift force. Our results suggest that a frequency of 5 Hz induces a $(C_L/C_D)_{max}$ ratio of 31.8, constituting a 158% gain over a flapping frequency of 4 Hz. This finding seems to support the hypothesis that a higher flapping frequency would compensate for some of the decrease in lift force, while maintaining a value of the L/D ratio that ensures a limited energy cost of high-altitude flight. Ultimately, this study improves our understanding of the biomechanical mechanisms adopted by migratory birds as they attempt to maintain a favorable balance between high-altitude flight and the energy cost associated with migration.

SUPPLEMENTARY MATERIAL

See the supplementary material for study limitations and a statement on uncertainty of results.

AUTHOR DECLARATIONS
Conflict of Interest

The authors have no conflict to disclose.

DATA AVAILABILITY

The data that support the findings of this study are available from the corresponding author upon reasonable request.

REFERENCES

[1]B. A. Cooper and R. J. Ritchie, "The altitude of bird migration in east-central Alaska: A radar and visual study," J. Field Ornithol. **66**, 590–608 (1995).
[2]F. Liechti and E. Schaller, "The use of low-level jets by migrating birds," Naturwissenschaften **86**, 549–551 (1999).
[3]J. M. V. Rayner, "Form and function in avian flight," in *Current Ornithology*, edited by R. F. Johnston (Springer, Boston, MA, 1988), Vol. 5.
[4]C. J. Pennycuick, "Mechanics of flight," Avian Biol. **5**, 1–75 (1975).
[5]U. M. Norberg, "Vertebrate flight: Mechanics," in *Physiology, Morphology, Ecology and Evolution* (Springer-Verlag, Berlin/Heidelberg, 1990).
[6]J. Rayner, P. Viscardi, S. Ward, and J. Speakman, "Aerodynamics and energetics of intermittent flight in birds," Am. Zool. **41**, 188–204 (2001).
[7]C. J. Pennycuick, "Speeds and wingbeat frequencies of migrating birds compared with calculated benchmarks," J. Exp. Biol. **204**, 3283–3294 (2001).
[8]C. M. Bishop *et al.*, "The roller coaster flight strategy of bar-headed geese conserves energy during Himalayan migrations," Science **347**, 250–254 (2015).

[9]A. Hedenström, T. Alerstam, M. Green, and G. Gudmundsson, "Adaptive variation of airspeed in relation to wind, altitude and climb rate by migrating birds in the Arctic," Behav. Ecol. Sociobiol. **52**, 308 (2002).

[10]C. J. Pennycuick, "Predicting wingbeat frequency and wavelength of birds," J. Exp. Biol. **150**, 171–185 (1990).

[11]C. Pennycuick, "Wingbeat frequency of birds in steady cruising flight: New data and improved predictions," J. Exp. Biol. **199**, 1613–1618 (1996).

[12]V. A. Tucker, "Respiratory physiology of house sparrows in relation to high-altitude flight," J. Exp. Biol. **48**, 55–66 (1968).

[13]A. Nafi, H. Ben-Gida, C. G. Guglielmo, and R. Gurka, "Aerodynamic forces acting on birds during flight: A comparative study of a shorebird, songbird and a strigiform," Exp. Therm. Fluid Sci. **113**, 110018 (2020).

[14]J.-S. Maeng, J.-H. Park, S.-M. Jang, and S.-Y. Han, "A modeling approach to energy savings of flying Canada geese using computational fluid dynamics," J. Theor. Biol. **320**, 76–85 (2013).

[15]T. Barber, "Aerodynamic ground effect: A case study of the integration of CFD and experiments," Int. J. Veh. Des. **40**, 299 (2006).

[16]N. Vandenberghe, S. Childress, and J. Zhang, "On unidirectional flight of a free flapping wing," Phys. Fluids **18**, 014102 (2006).

[17]H. Bao, B. Song, W. Yang, and D. Xue, "The function of the alula with different geometric parameters on the flapping wing," Phys. Fluids **33**, 101907 (2021).

[18]X. Meng, "Ceiling effects on the aerodynamics of a flapping wing at hovering condition," Phys. Fluids **31**, 051905 (2019).

[19]J. Song, "Fly low: The ground effect of a barn owl (*Tyto alba*) in gliding flight," Proc. Inst. Mech. Eng., Part C **235**, 308–318 (2021).

[20]F. Beaumont, R. Taiar, G. Polidori, H. Trenchard, and F. Grappe, "Aerodynamic study of time-trial helmets in cycling racing using CFD analysis," J. Biomech. **67**, 1–8 (2018).

[21]G. Polidori, F. Legrand, F. Bogard, F. Madaci, and F. Beaumont, "Numerical investigation of the impact of Kenenisa Bekele's cooperative drafting strategy on its running power during the 2019 Berlin marathon," J. Biomech. **107**, 109854 (2020).

[22]D. L. Altshuler, J. W. Bahlman, R. Dakin, A. H. Gaede, B. Goller, D. Lentink, P. S. Segre, and D. A. Skandalis, "The biophysics of bird flight: Functional relationships integrate aerodynamics, morphology, kinematics, muscles, and sensors," Can. J. Zool. **93**, 961–975 (2015).

[23]J. M. V. Rayner, "A new approach to animal flight mechanics," J. Exp. Biol. **80**, 17–54 (1979).

[24]T. Liu, K. Kuykendoll, R. Rhew, and S. Jones, "Avian wings," AIAA Paper No. 2004-2186, 2004.

[25]G. Dimitriadis, J. D. Gardiner, P. G. Tickle, J. Codd, and R. L. Nudds, "Experimental and numerical study of the flight of geese," Aeronaut. J. **119**, 803–832 (2015).

[26]B. Blocken, "Computational fluid dynamics for urban physics: Importance, scales, possibilities, limitations and ten tips and tricks towards accurate and reliable simulations," Build. Environ. **91**, 219–245 (2015).

[27]G. D. Funk, W. K. Milsom, and J. D. Steeves, "Coordination of wingbeat and respiration in the Canada goose. I. Passive wing flapping," J. Appl. Physiol. **73**, 1014–1024 (1992).

[28]L. L. Gould and F. Heppner, "The vee formation of Canada geese," Auk **91**, 494–506 (1974).

[29]P. Chai, et and R. Dudley, "Limits to flight energetics of hummingbirds hovering in hypodense and hypoxic gas mixtures," J. Exp. Biol. **199**, 2285–2295 (1996).

[30]P. Chai, R. Harrykissoon, and R. Dudley, "Hummingbird hovering performance in hyperoxic heliox: Effects of body mass and sex," J. Exp. Biol. **199**, 2745–2755 (1996).

[31]T. Defraeye, B. Blocken, E. Koninckx, P. Hespel, and J. Carmeliet, "Computational fluid dynamics analysis of cyclist aerodynamics: Performance of different turbulence-modelling and boundary-layer modelling approaches," J. Biomech. **43**, 2281–2287 (2010).

[32]S. G. Chefranov and A. S. Chefranov, "The new exact solution of the compressible 3D Navier–Stokes equations," Commun. Nonlinear Sci. Numer. Simul. **83**, 105118 (2020).

[33]F. Menter, "Zonal two equation k-w turbulence models for aerodynamic flows," AIAA Paper No. 1993-2906, 1993.

[34]D. M. Fintelman, H. Hemida, M. Sterling, and F.-X. Li, "CFD simulations of the flow around a cyclist subjected to crosswinds," J. Wind Eng. Ind. Aerodyn. **144**, 31–41 (2015).

[35]J. Song, B. Tobalske, D. R. Powers, T. Hedrick, and H. Luo, "Three-dimensional simulation for fast forward flight of a calliope hummingbird," Roy. Soc. Open Sci. **3**, 160230 (2016).

[36]R. Dvořák, "Aerodynamics of bird flight," EPJ Web Conf. **114**, 01001 (2016).

[37]J. Kweon and H. Choi, "Sectional lift coefficient of a flapping wing in hovering motion," Phys. Fluids **22**, 071703 (2010).

[38]S. F. Hoerner and H. V. Borst, *Fluid-Dynamic Lift: Practical Information on Aerodynamic and Hydrodynamic Lift* (LA Hoerner, 1985).

[39]P. C. Withers, "An aerodynamic analysis of bird wings as fixed aerofoils," J. Exp. Biol. **90**, 143–162 (1981).

[40]A. Martín-Alcántara, R. Fernandez-Feria, and E. Sanmiguel-Rojas, "Vortex flow structures and interactions for the optimum thrust efficiency of a heaving airfoil at different mean angles of attack," Phys. Fluids **27**, 073602 (2015).

[41]H. Schmaljohann and F. Liechti, "Adjustments of wingbeat frequency and air speed to air density in free-flying migratory birds," J. Exp. Biol. **212**, 3633–3642 (2009).